Repression of ferritin light chain translation by human eIF3

Authors: Mia C. Pulos-Holmes[1], Daniel N. Srole[1†], Amy S. Y. Lee[2], Maria G. Juarez[1], David T. McSwiggen[1], Nicholas T. Ingolia[1,4], Jamie H. D. Cate[1,3,4,5,*]

[1] Department of Molecular & Cell Biology, University of California, Berkeley, California 94720, USA.

[2] Biology Department, Rosenstiel Basic Medical Science Research Center, Brandeis University, Waltham, Massachusetts, 02454, USA

[3] Department of Chemistry, University of California, Berkeley, California 94720, USA.

[4] California Institute for Quantitative Biosciences 3 (QB3), University of California, Berkeley, California 94720, USA.

[5] *Molecular Biophysics* & *Integrated Bioimaging* Division, Lawrence Berkeley National Laboratory, Berkeley, California 94720, USA.

[†] Present address: *Department of Molecular & Medical Pharmacology*, David Geffen School of Medicine at UCLA, University of California Los Angeles, Los Angeles, California 90095, USA.

* Corresponding author: Jamie H. D. Cate[1,3,4,5] jcate@lbl.gov

Abstract: A central problem in human biology remains the discovery of causal molecular links between mutations identified in genome-wide association studies (GWAS) and their corresponding disease traits. This challenge is magnified for variants residing in non-coding regions of the genome. Single-nucleotide polymorphisms (SNPs) in the 5' untranslated region (5'-UTR) of the ferritin light chain (*FTL*) gene that cause hyperferritinemia are thought to disrupt translation repression by altering iron regulatory protein (IRP) interactions with the *FTL* mRNA 5'-UTR. Here, we show that human eukaryotic translation initiation factor 3 (eIF3) acts as a distinct repressor of *FTL* mRNA translation, and eIF3-mediated *FTL* repression is disrupted by a subset of SNPs in *FTL* that cause hyperferritinemia. These results identify a direct role for eIF3-mediated translational control in a specific human disease.

INTRODUCTION

Iron is essential for a spectrum of metabolic pathways and cellular growth. However, if not properly managed, excess iron catalyzes the production of reactive oxygen species (ROS). To safeguard against these toxic effects, cells sequester iron in ferritin, a cage-like protein complex composed of a variable mixture of two structurally similar but functionally distinct subunits, the ferritin heavy chain (FTH) and the ferritin light chain (FTL) (Harrison and Arosio, 1996),(Knovich et al., 2009). To maintain iron homeostasis, the expression of both ferritin subunits in mammals is regulated post-transcriptionally by iron regulatory proteins that bind a highly conserved RNA hairpin called the iron responsive element (IRE), located in the 5'-UTRs of *FTL* and *FTH1* mRNAs (Figure 1A, 1B) (Theil, 1994),(Wilkinson and Pantopoulos, 2014). SNPs or deletions in the 5'-UTR that disrupt IRP-IRE interactions are thought to be the primary cause of hereditary hyperferritinemia cataract syndrome, a condition involving an abnormal buildup of serum ferritin in the absence of iron overload (Cazzola et al., 1997).

Although the IRP-IRE interactions have been considered to be the sole post-transcriptional means of regulating ferritin expression, recent studies have provided strong evidence that other presently-unknown factors may provide another layer of regulation during *FTL* translation. For example, the FTL subunit composition of ferritin is altered in response to environmental factors such as hypoxia (Sammarco et al., 2008). We recently found that eIF3 can function beyond its scaffolding role in general

translation initiation by acting as either an activator or repressor of translation in a transcript-specific manner (Lee et al., 2015),(Lee et al., 2016). This regulation occurs through interactions with primarily 5'-UTR RNA structural elements (Lee et al., 2015). Notably, we found that *FTL* mRNA cross-links to eIF3 (Lee et al., 2015), but the role eIF3 plays in regulating *FTL* translation has not been established.

Here we report a previously unknown mode of *FTL* translation regulation with a direct link to disease-related genetic mutations. We show that eIF3 binds to human *FTL* mRNA by means of sequences in the 5'-UTR immediately adjacent to the IRE, and provides additional regulation of *FTL* translation independent of IRP-IRE. After using CRISPR-Cas9 genome editing to delete the endogenous eIF3 interaction site in *FTL*, we monitored direct phenotypic responses of cells under normal and iron modulated conditions. Lastly, we used competitive IRP binding assays to explore the potential role of eIF3 in hyperferritinemia. These experiments reveal that eIF3 acts as a repressor of *FTL* translation, and disruption of eIF3 interactions with *FTL* mRNA due to specific SNPs in the *FTL* 5'-UTR likely contributes to a subset of hyperferritinemia cases.

RESULTS

Identification of the eIF3-*FTL* mRNA interaction site

In order to understand the functional effect of the interaction between eIF3 and *FTL* mRNA, we utilized *Renilla* luciferase (rLuc) reporter mRNAs in which the 5'-UTR from *FTL* was placed upstream of the *Renilla* coding sequence (Figure 1C). To measure

the importance of the *FTL* mRNA region identified by PAR-CLIP (Lee et al., 2015), various mutations were introduced into the *FTL* 5'-UTR to disrupt eIF3 binding. The eIF3 binding site on the 5'-UTR of *FTL*, as determined by PAR-CLIP, spans a 24 nucleotide sequence within a secondary structural element that overlaps with the last five nucleotides of the annotated sequence of the *FTL* IRE (Figure 1 – figure supplement 1). Notably, no eIF3 cross-linking site was observed in the 5'-UTR of the mRNA encoding *FTH1,* which shares the structurally conserved IRE, but not adjacent sequence features (Figure 1 – figure supplement 1B) (*7*). The removal of the eIF3 interaction site dramatically increased translation of rLuc when compared to the full length wild type *FTL* 5'-UTR, 93-fold when the PAR-CLIP defined sequence was deleted (Δ*PAR,* nucleotides 53-76) and 12-fold in a deletion the maintained the full IRE sequence (eIF3 repressive element, Δ*3RE*, nucleotides 58-90) (Figure 1D, 1E) (Theil, 2015). These results suggest that eIF3 binding to the *FTL* 5'-UTR represses *FTL* translation.

Decoupling the repressive role of eIF3 on *FTL* mRNA from that of IRP

Due to the close proximity between the eIF3 interaction site and the *FTL* IRE, accompanied by the fact that the 5'-UTR of *FTL* is prone to large-scale structural rearrangements (Martin et al., 2012), we tested whether the derepression observed in the Δ*PAR* and Δ*3RE* mRNAs is a direct result of altering eIF3 binding and not due to disrupting the IRE-IRP interaction. To evaluate the effect of the deletions (Δ*PAR,* Δ*3RE*) on IRP binding, we carried out RNA-electrophoretic mobility shift assays with near-IR labeled *FTL* 5'-UTR RNA and recombinant IRP1. As expected, IRP1 bound to the wild

type 5'-UTR of *FTL* (Figure 2A). IRP1 also bound the Δ*3RE* RNA, but failed to bind efficiently to the Δ*PAR* RNA (Figure 2A). The loss of IRP1 binding to Δ*PAR* RNA could be attributed to disrupted RNA folding, or to the importance of the region of overlap between the IRE and the PAR-CLIP defined eIF3 binding site (Figure 1 – figure supplement 1C). We further quantified IRP binding to the Δ*3RE* 5'-UTR using RNA binding competition assays (Figure 2B, 2C, Figure 2 – figure supplement 1). IRP1 had slightly attenuated binding to the Δ*3RE* 5'-UTR RNA when compared to the wild type *FTL* 5'-UTR, suggesting that the alleviation of repression observed in the luciferase translation experiments for the Δ*3RE* mRNA (Figure 1E) could be due to disruption of eIF3 binding.

To further ensure that the alleviation of repression of *FTL* translation by the Δ*3RE* mutation results primarily from disruption of eIF3-*FTL* binding and not IRE-IRP interactions, we modulated the location of the IRE in the 5'-UTR of *FTL*. It had been shown previously that moving the IRE in the *FTH1* 5'-UTR further than 60 nucleotides from the 5' m^7G-cap partially relieves IRP-dependent inhibition of *FTH1* translation (Goossen and Hentze, 1992). Inhibition is lost because bound IRP can no longer sterically block the assembly of the 43S preinitiation complex on the mRNA (Muckenthaler et al., 1998),(Paraskeva et al., 1999). To further investigate if this holds for *FTL* mRNA, we used the *FTL* and Δ*3RE* luciferase reporter constructs and placed the characteristic C bulge of the IRE either 32 nucleotides away (native) or 70 nucleotides away (extended) from the 5' cap (Figure 2D). As with *FTH1* mRNA, moving the IRE further from the 5' cap derepressed translation of the *FTL*-based luciferase

reporter (Figure 2E). Notably, overall translation was much higher from both Δ*3RE* mRNAs, even with removal of IRP-dependent repression due to the distance from the 5'-cap (Figure 2E). This cap position-independent derepression is unique to *FTL* as the 3RE region is not conserved in the *FTH1* 5'-UTR. Furthermore, combining the Δ*3RE* mutation with a mutation that disrupts IRP binding to the IRE entirely (Loop) (Cazzola et al., 1997) synergistically derepressed luciferase reporter translation (Figure 2F). Taken together, these results indicate that IRP-mediated inhibition of translation is maintained in the Δ*3RE* mRNA, and that eIF3 confers an additional level of repression beyond that which can be provided by IRP.

We used the luciferase reporter results in Figure 2F to formulate a mathematical model to determine whether eIF3 and IRP can bind *FTL* mRNA simultaneously (See methods for details). We defined a system in which IRP and eIF3 do not bind the same mRNA. This leaves three possible states in which the *FTL* mRNA could exist: the fraction bound solely by IRP (x_1), the fraction bound solely by eIF3 (x_2), and the remainder of the mRNA which is unbound by either factor (x_3) (Figure 2 – figure supplement 2). We further elaborated this model to include translation efficiency (y). Here we assume the mutations do not affect the translation efficiency of the unbound species (x_3), while the other two populations (x_1 and x_2) have translational efficiencies (y_1 and y_2) scaled between full repression ($y_n = 0$) and no repression ($y_n = 1$). Lastly, we assumed the mutations that disrupt binding shift the equilibrium of the total mRNA population between bound and unbound fractions of the alternate factor by some amount, either α for those affecting eIF3 binding or β for IRP binding. Using the

translational output determined in Figure 2F, we find that the data are inconsistent with the model that eIF3 and IRP cannot bind the same mRNA. Rather, the data indicate that IRP and eIF3 likely act in *cis* on at least a fraction of the *FTL* mRNA.

Physiological response to loss of eIF3-dependent repression

To investigate the physiological response to the loss of eIF3-based repression, we genetically engineered either HEK293T or HepG2 cells to generate the Δ*3RE* mutation in the 5'-UTR in the *FTL* gene (Figure 3 – figure supplement 1A-1C). Notably, we found that the Δ*3RE* mutation abolished the preferential interaction of eIF3 with *FTL* mRNA (Figure 3 – figure supplement 1D, 1E). Furthermore, FTL protein production increased dramatically in the Δ*3RE* cell lines, as expected from removing the predicted eIF3 repressive element (Figure 3A). Importantly, the increase in FTL protein levels was not due to increases in mRNA levels (Figure 3 – figure supplement 2A), indicating that the de-repression occurs post-transcriptionally. Remarkably, the increase in FTL levels occurs with a concurrent reduction in FTH levels (Figure 3B). The decrease in FTH protein levels is also not due to changes in *FTH1* mRNA levels (Figure 3 – figure supplement 2B).

To ensure that IRP-mediated repression was maintained in the Δ*3RE* cell lines, we transiently transfected the WT and Δ*3RE* cell lines with plasmids encoding C-terminally FLAG-tagged IRP. We then used FLAG immunoprecipitation followed by qPCR to determine whether IRP is bound to the edited *FTL* and other IRE containing

mRNAs *in vivo*. We found that FLAG-tagged IRP bound *FTL* mRNA similarly in the wild type and Δ*3RE* cell line (Figure 3C). Intriguingly, *FTH1* mRNA was recovered at a significantly higher level in the Δ*3RE* cell line compared to wild type cells (Figure 3C), suggesting increased IRP binding. This increased binding of IRP to *FTH1* mRNA may explain the concurrent decrease in FTH abundance seen in Figure 3B.

To test whether IRP maintains its ability to dynamically regulate *FTL* translation, we treated the cell lines with either ferric ammonium citrate (FAC), an iron donor, or desferoxamine (DFO), an iron chelator, to increase or decrease iron levels, respectively. (Figure 3 – figure supplement 3) (Schneider and Leibold, 2003). FTL levels in the Δ*3RE* cell lines responded to FAC and DFO treatment in a comparable manner to the unedited (WT) cell lines (Figure 3D), showing that the Δ*3RE* transcript retains IRP-dependent translational regulation in cells. This iron-responsive regulation is maintained even though the basal levels of FTL protein are much higher in the Δ*3RE* compared to WT cells (Figure 3D). FTH levels also respond to iron levels in both the WT and Δ*3RE* cells (Figure 3 – figure supplement 3), with basal FTH levels reduced in the Δ*3RE* compared to WT cells. Taken together, these data further support the hypothesis that the observed de-repression in the Δ*3RE* cells is due to the modulation of eIF3-based regulation of *FTL* translation, and not due to disruption of IRP-mediated regulation.

We proceeded to investigate whether the lack of eIF3-based repression of *FTL* translation and concomitant decrease in FTH protein levels had any effects on the assembled ferritin complexes. We purified the ferritin complexes from either wild-type

HepG2 cells or the Δ*3RE* cell line using a fractional methanol precipitation protocol (Cham et al., 1985). We observed that the Δ*3RE* cell line not only had eight-fold more ferritin complex compared to wild-type HepG2 cells, but this complex was far more stable. Without ferric ammonium citrate (FAC) treatment to stabilize the complex (Linder, 2013), ferritin purified from WT cells consistently degraded, unlike the stable complexes from the Δ*3RE* cell line (Figure 3 – figure supplement 4). This implicates eIF3 in regulating not only the abundance of the two ferritin subunits, but also the dynamics and stability of the ferritin complex. Taken together, these results support the hypothesis that removal of the eIF3 interaction site in the 5'-UTR of the *FTL* mRNA derepresses *FTL* translation and can have a dramatic effect on ferritin subunit composition in the cell.

SNPs in *FTL* that cause hyperferritinemia

Although the Δ*3RE* mutation in *FTL* revealed eIF3-dependent repression of *FTL* translation, it is not clear what role eIF3 may play in ferritin homeostasis in humans. The human genetic disease hereditary hyperferritinemia cataract syndrome (HHCS) is an autosomal dominant condition that primarily results in early onset of cataracts due to ferritin amassing in the lens (Millonig et al., 2010). HHCS arises from SNPs or deletions in the 5'-UTR of *FTL*, which are thought to disrupt the IRP-IRE interaction leading to increased *FTL* translation. For example, mutations observed in the apical loop of the IRE directly disrupt critical contacts essential for IRP binding to the IRE (Figure 4A) (5).

Interestingly, two SNPs identified in certain patients with hyperferritinemia, G51C and G52C, disrupt the nucleotides one and two bases upstream of the annotated eIF3 PAR-CLIP site (Figure 4A) (Camaschella et al., 2000),(Luscieti et al., 2013). Although the PAR-CLIP methodology maps the region of interaction between an RNA and protein of interest, it does not always capture the full interaction site due to the requirement for 4-thiouridine cross-linking and subsequent RNase digestion to generate fragments for deep sequencing (Ascano et al., 2011), (Hafner et al., 2010).Thus, we wondered whether the G51C and G52C SNPs could potentially impact eIF3 repression of *FTL* mRNA translation, due to the proximity of the G51C and G52C mutations to the eIF3 PAR-CLIP site. We generated luciferase reporter constructs with either of the G51C and G52C SNPs, as well as a control with the previously described mutations in the IRE apical loop, and used mRNA transfections to test their effects on luciferase translation levels. All mutations led to an increase in luciferase levels, indicating that they alleviated translational repression (Figure 4B). We also observed that the G51C and G52C mRNAs do not interact with eIF3, based on eIF3 immunoprecipitations from transfected HEK293T cells (Figure 4C). Furthermore, the G51C and G52C SNPs maintained near wild-type IRP binding (Figure 4D, 4E), in stark contrast to the mutations in the IRE apical loop (Figure 4A), which completely abolished the interaction between IRP1 and the 5'-UTR element (Figure 4 – figure supplement 1). These results identify SNPs in *FTL* that cause hyperferritinemia due to disruption of eIF3-dependent repression of *FTL* translation.

DISCUSSION

We have shown that eIF3 represses the translation of *FTL* mRNA by binding a region of the *FTL* 5'-UTR immediately adjacent to the IRE. Upon disruption of eIF3 binding, the basal level of FTL production increases dramatically without affecting the iron-responsiveness of *FTL* translation (Figure 3), or binding of IRP to the remainder of the 5'-UTR containing the IRE (Figure 2, Figure 3, Figure 4). Taken together, these results expand the classical model of *FTL* mRNA post-transcriptional regulation by the iron-responsive IRP/IRE interaction to include a functionally distinct eIF3-dependent repressive mechanism (Figure 5). The physiological need for a dual repressive system involving IRPs and eIF3 in normal human health remains to be determined. Experiments combining the Δ*3RE* and apical loop mutations (Figure 2F, Figure 2 – figure supplement 2) suggest that eIF3 and IRP can act simultaneously to repress *FTL* translation. Due to the close proximity of the IRE and eIF3 binding sites, and as suggested by our mathematical modeling (Figure 2 – figure supplement 2), it may be possible that eIF3 physically interacts with IRP when they bind to the 5'-UTR in *FTL* mRNA in certain tissue or cellular contexts.

Our present findings also provide the first molecular evidence for the direct involvement of eIF3 in a human disease caused by SNPs in the human population. We found that disruption of eIF3-mediated regulation of *FTL* translation could serve as the dominant cause of certain cases of hyperferritinemia. The specific genetic mutations we analyzed (G51C, G52C) map to the less-conserved lower stem of the IRE, and are predicted to have no direct physical interaction with IRP1 (PDB: 3SNP) (Walden et al.,

2006). Here, we establish that these mutations minimally interfere with IRP's interaction with the IRE, whereas they greatly impact the eIF3-based interaction and *FTL* translational repression (Figure 4C-E). This work highlights how even highly clustered SNPs can contribute to disease through divergent molecular mechanisms. In the case of *FTL*, these clustered SNPs can disrupt three different aspects of translation regulation: IRP binding, eIF3 binding, or RNA folding (Figure 5).

While our results connect eIF3 translational control to specific examples of hyperferritinemia, they also suggest a broader role for eIF3 in other hyperferritinemias and ferritin-related diseases. For example, we observed that derepression of *FTL* translation by disruption of the eIF3 interaction site leads to a concomitant decrease in FTH levels, driving an overall increase in ferritin complex abundance and stability (Figure 3 – figure supplement 4). Ferritin is a known mediator of inflammatory responses, raising the question of whether eIF3 may contribute to ferritin's role in inflammation (Morikawa et al., 2009),(Recalcati et al., 2008). Our results provide new insights that should help connect molecular mechanisms of translational control to disease-associated SNPs identified in ever expanding genomic databases.

Materials and Methods:

Plasmids

The *FTL* 5'-UTR was amplified from human cDNA, and cloned into the pcDNA4 vector with a modified Kozak sequence (Kranzusch et al., 2014), by using In-Fusion® HD Cloning Kit (Takara, Cat.# 638911) to generate the starting luciferase reporter

plasmids. The *FTL* transcription start site is derived from the FANTOM5 database (Lizio et al., 2015). Additional mutations were generated through around-the-horn cloning using either blunt primers for deleting regions or primers with overhangs to introduce single or double nucleotide mutations. The IRP1 protein expression plasmid was generated by amplifying the human IRP1 sequence from human cDNA and inserting it into the 2B-T vector (Addgene, plasmid # 29666) following a His_6 tag and TEV protease cleavage site. The IRP-FLAG construct was generated by inserting a 1X FLAG tag at the C-terminal end of IRP in the pCMV6-XL4 backbone (OriGENE, SC126974).

***In vitro* transcription**

RNAs were transcribed using T7 RNA polymerase prepared in-house. For luciferase reporter mRNAs, 5'-capping and 3'-polyadenylation were performed co-transcriptionally by including 3´-O-Me-m ^{7}G(5´)ppp(5´)G RNA Cap Structure Analog (NEB, Cat.# S1411L) and using linearized plasmid template that had a sequence encoding a poly-A tail. Non-labeled RNAs for the IRP1 electrophoresis mobility shift assays were generated in the same manner, except the templates were not polyadenylated. Additionally, RNAs with the 38-nucleotide extension between the 5' -cap and IRE were constructed using a random nucleotide sequence. The exact nucleotide composition 5' of the IRE was previously reported to not significantly impact IRP binding (Goossen and Hentze, 1992). RNAs were purified after DNA template digestion by phenol-chloroform extraction and ethanol precipitation.

For genome editing, we used tandem CRISPR-Cas9 enzymes programmed with single-guide RNAs (sgRNAs) targeting the *FTL* gene, along with a single stranded DNA

(ssDNA) oligonucleotide homologous to the regions spanning the deleted 3RE sequence (Figure 3 - figure supplement 1). sgRNAs were designed using the CRISPR.MIT.EDU program from the Feng Zhang Lab, MIT. CRISPR-Cas9-sgRNA was assembled as RNA-protein complexes (RNPs) (Kim et al., 2014). The DNA for transcription was synthesized by appending the sgRNA sequence downstream of a T7 RNA polymerase promoter. The DNA was then purified using phenol-chloroform extraction followed by isopropanol precipitation. After transcription, the RNA products were treated with DNase I (Promega, Cat.# M6101), run on a 10% denaturing polyacrylamide gel (6 M urea), and extracted from the gel using the crush and soak method and ethanol precipitation.

Luciferase reporter transfections

Human HepG2 cells were maintained in DMEM (Invitrogen 11995-073) with 10% FBS (Seradigm) and 1% Pen/Strep (Gibco, Cat.# 15140122). Transfections of the luciferase reporter mRNAs were done using the Mirus *Trans*IT®-mRNA Transfection Kit (Cat.# MIR 2250), with the following protocol modifications. The day prior to transfection, HepG2 cells were seeded into opaque 96-well plates so that they would reach 80% confluence at the time of transfection. At this point, 200 ng of 5'-capped and 3'-polyadenylated mRNA was added at room temperature to OptiMEM media (Invitrogen, Cat.# 31985-088) to a final volume of 10 µL. Then, 0.6 µL of both Boost reagent and TransIT mRNA reagent were added to the reaction and left to incubate at room temperature for 3 min. The TransIT-mRNA Reagent:mRNA Boost:RNA complex was distributed to the cells in a drop wise manner. Luciferase activity was assayed either 6 hr, 8 hr, or 18 hr post-transfection using the *Renilla* Luciferase assay kit

(Promega, Cat.# E2820) and a Microplate Luminometer (Veritas). The shorter (6 hr) incubation between transfection and luciferase readout was used for data seen in Figure 2F in order to avoid saturating the luciferase signal.

Cell line generation

To generate *FTL*-eIF3 interaction site null cell lines (Δ3RE), we used tandem CRISPR-Cas9 enzymes programmed with single-guide RNAs (sgRNAs) targeting the *FTL* gene, along with a single-stranded DNA (ssDNA) donor with homology to the regions spanning the deleted Δ3RE sequence. The sgRNAs were generated as described above, and targeted regions on both sides of the eIF3 interaction site (Figure 2A). The RNP complex was generated by incubating 100 pmol Cas9 with the two sgRNAs at a 1:1.2 Cas9 to total sgRNA ratio. This mixture was heated to 37 °C for 10 min and then kept at room temperature until use. The ssDNA donor was 90 nucleotides long, with 45-nucleotide homology on either side of the predicted double-strand cut sites allowing it to have perfect homology to the predicted edited sequence.

The Cas9-sgRNA RNP complexes, along with 500 pmol of the ssDNA donor, were transfected into either $5x10^5$ HEK293T or HepG2 cells using the Lonza 96 well shuttle system SF kit (Cat. # V4SC-2096). The nucleofection programs used were as follows: CM-130 for HEK293T and EH-100 for HepG2. The transfected cells were left to incubate for either 48 hrs for HEK293T cells or 72 hrs for HepG2 cells before harvesting and extracting gDNA using QuickExtract (Epicentre: QE09060). The editing efficiency of individual Cas9-sgRNA RNPs was determined using a T7 endonuclease 1 assay

(Reyon et al., 2012). The efficiency of the dual-sgRNA editing approach was determined by PCR-amplifying a 180-base pair region around the eIF3 interaction site, and analyzing the resulting products on a 6% non-denaturing 29:1 polyacrylamide gel. This method achieved an editing efficiency of nearly 100% in HEK293T cells and roughly 85% in HepG2 cells (Figure 3 – figure supplement 1B). Monoclonal populations of edited cells were sorted using FACS, screened, and the final edited sequence was determined using TOPO TA cloning (Ramlee et al., 2018).

Transcript level abundance

Total transcript abundance was determined by lysing 1.25 x 10^6 cells with Qiazol lysis buffer followed by using the Directzol RNA extraction kit (Zymo Research, Cat. # R2061), according to the manufacturer's instructions. The cDNA was generated by reverse transcription using 350 ng of RNA, random hexamers, and Superscript IV (Thermo Fisher scientific, Cat. # 18091050). Primers for the qPCR were as follows: FTL forward: 5' -ACCTCTCTCTGGGCTTCTAT-3', FTL reverse: 5' -AGCTGGCTTCTTGATGTCCT-3' (Cozzi et al., 2004), ACTB forward: 5'-CTCTTCCAGCCTTCCTTCCT-3', ACTB reverse: 5'-AGCACTGTGTTGGCGTACAG-3' (Chen et al., 2008), PSMB6 forward: 5'-GGACTCCAGAACAACCACTG-3', PSMB6 reverse: 5'-CAGCTGAGCCTGAGCGACA-3' (Mokany et al., 2013), FTH1 forward: 5'-CGCCAGAACTACCACCA-3', FTH1 reverse: 5'-TTCAAAGCCACATCATCG-3' (Liu et al., 2012),18S forward: 5'-GGCCCTGTAATTGGAATGAGTC-3', 18S reverse: 5'-CCAAGATCCAACTACGAGCTT-3' (Lee et al., 2016), RLUC forward: 5’-GGAATTATAATGCTTATCTACGTGC-3', RLUC reverse: 5'-

CTTGCGAAAAATGAAGACCTTTTAC-3' (Kong et al., 2008). Run conditions were: 95˚C for 15 sec, followed by 40 cycles of 95˚C for 15 sec, 60˚C for 60 sec, 95˚C for 1 sec.

RNA immunoprecipitation and qPCR

The EIF3B-RNA immunoprecipitations were adapted from (Lee et al., 2015) with the following modifications. One 15 cm plate of either HEK293 or HepG2 cells was used to prepare cell lysate using a NP40 lysis buffer (50 mM HEPES-KOH pH 7.5, 150 mM KCl, 2 mM EDTA, 0.5% Nonidet P-40 alternative, 0.5 mM DTT, 1 Complete EDTA-free Proteinase Inhibitor Cocktail tablet per 50 mL of buffer). The lysate was precleared with 15 µL of Dynabeads preloaded with rabbit IgG (Cell Signaling, Cat. # 2729) for one hour at 4 °C. The lysate was collected and then incubated with a fresh 15 µL aliquot of Dynabeads and 7.5 µL of anti-EIF3B antibody (Bethyl A301-761A) for two hours at 4 °C. Preparation of cDNA and qPCR primers are described and listed above.

For EIF3B immunoprecipitations of transfected mRNAs, 2.15 µg of mRNA was transfected into 1 well of either HEK293T or HepG2 cells in a 12-well plate using the protocol above. Cells were then left to incubate for 8 hours before harvesting. The cells were lysed using the NP40 lysis buffer listed above (Lee et al., 2015), and precleared with 2 µL of rabbit IgG-coated Dynabeads for one hour at 4 °C. The lysate was collected and then incubated with a fresh 2 µL aliquot of Dynabeads and 4 µL of anti-EIF3B antibody (Bethyl A301-761A) for two hours at 4 °C. RNA was collected, cDNA prepared and qPCR carried out with the primers and run conditions as described in the methods for transcript level abundance.

For FLAG-tagged IRP1 immunoprecipitations, 2.2 µg of plasmid DNA was transfected into a 10 cm dish of 80% confluent HEK239T WT cells or HEK293T Δ*3RE* mutant cells. Cells were then left to incubate for 24 hours before harvesting. The cells were lysed using the NP40 lysis buffer as described in (Lee et al., 2015) and then further diluted 3x with the lysis buffer lacking DTT. The lysate was collected and then incubated with pre-equilibrated anti-FLAG antibody conjugated agarose beads (Sigma A2220) for two hours at 4 °C. The beads were then washed with a high salt wash buffer (50 mM HEPES-KOH pH 7.5, 300 mM KCl, 2 mM EDTA, 1% Nonidet P-40 alternative) three times. The protein was eluted from the beads using two washes with 1X FLAG peptide for 30 min each at 4 ˚C. The RNA was collected using phenol/chloroform extraction followed by ethanol precipitation. cDNA was prepared using Superscript IV (Thermo Fisher scientific, Cat. # 18091050) and qPCR carried out with the primers and run conditions as described above in the methods for determination of transcript level abundance.

Iron level modulation and ROS treatment

In order to modulate the iron levels in cells, HepG2 and HEK293T cells were treated with a final concentration of either 50 µg/mL of ferric ammonium citrate (FAC) (an iron donor) for 24 hours or either 200 µM for 24 hours or 50 µM for 48 hours of desferoxamin (DFO) (an iron chelator) before harvesting.

IRP1 purification

IRP1 was purified based on the protocols in (Carvalho and Meneghini, 2008), (Basilion et al., 1994) with modifications. The IRP1-encoding 2B-T plasmid was

transformed into chemically-competent BL21 Rosetta pLysS *E. coli*, using heat shock at 42 °C, and grown on Ampicillin plates. A single colony was used to inoculate a 5 mL LB culture containing Ampicillin, which was then used to inoculate a 50 mL starter culture that was allowed to reach saturation overnight. Approximately 4x10 mL of the overnight culture was used to inoculate 4x1L cultures using ZY5052 media lacking the 1000x trace metal mix (30mM HEPES, 5% glycerol, 43mM KCl, 0.5mM EDTA, 0.5 mM DTT) (Studier, 2005) plus Carbomicillin. The 1 L cultures were grown at 37 °C to OD_{600} = 0.36, at which point the temperature was lowered to 18 °C, and allowed to grow at 18 °C for 36 hours prior to harvest.

Pelleted *E. coli* cells were lysed using sonication in lysis buffer (30 mM HEPES pH=7.5, 400 mM KCl, 5% Glycerol and 1 mM DTT) along with Protease inhibitor (Roche, Cat. # 5056489001) tablets. Lysate was loaded on a 5 mL Ni-NTA pre-packed HiTrap column (GE, Cat. # 17-5248-02), allowed to incubate at 4 °C for 1 hour, before eluting using 600 mM imidazole in the same buffer as above. Pooled fractions from the elution were then dialyzed overnight into ion-exchange (IEX) buffer (30 mM HEPES pH 7.5, 1 mM DTT, 5% Glycerol, and 1 mM EDTA), for subsequent purification using a 5 mL HiTrap Q-column (GE, Cat. # 17-1154-01). Samples were then loaded on a Q column using IEX buffer, and the column was washed with eight column volumes of IEX buffer without KCl. IRP1 was eluted using 800 mM KCl in IEX buffer.

IRP1 electrophoresis mobility shift assays

To detect IRP1 binding by native gel shifts, RNA samples were transcribed using the Atto-680 RNA Labeling Kit (Jena Bioscience, FP-220-680) and subsequently purified using RNA Clean & Concentrator-25 columns (Zymo, R1018). This form of labeling has been shown not to disrupt protein-RNA interactions (Kohn et al., 2010). Unlabeled RNA was transcribed and purified as described above.

Binding experiments were carried out with a final concentration of 300 pM of labeled RNA and 225 nM of recombinant human IRP1, which facilitated a 1:1 ratio of RNA binding to IRP1. We first ensured the RNA competition experiments reached equilibrium – which required at least 11 hours of incubation – by measuring the approximate dissociation rate constant (k_{off}) of WT *FTL* 5'-UTR from IRP1. Heparin was included at the beginning of the reaction at a final concentration of 4.5 µg/mL. The initial binding reaction was carried out in a 1x RXN buffer (40 mM KCl, 20 mM Tris-HCL, pH 7.4, 2 mM $MgCl_2$, 2 mM DTT, and 5% Glycerol) for 30 minutes at room temperature (Goforth et al., 2009),(Fillebeen et al., 2014). For competition experiments, unlabeled RNA was then added in concentrations 1000x-100,000x that of the labeled RNA. In preliminary experiments, we found the k_{off} to be roughly 0.006 min^{-1} using an 8-hour incubation time course with competitor. We then tested the fraction of IRP bound after 11 hr and 18 hr incubations with competitor *FTL* RNA and observed no changes in the residual fraction of IRP bound to RNA (~15%), indicating the reactions had reached equilibrium. Thus, subsequent experiments with competitor RNAs were carried out for 18 hr, after the first 30-minute pre-incubation in the absence of competitor. The

reactions were resolved on Tris-glycine gels (Thermo Fisher Scientific, Cat.# XP04122BOX) and gels was visualized using an Odyssey Licor set to 700 nM wavelength and an intensity of 6.5. Band intensity quantification was carried out using Image Studio (Licor). The IC_{50} values for each competitor RNA was determined using Graph Pad Prism 7 (Graph Pad Software) from a set of triplicate experiments, except for the Δ3RE competitor RNA, which was tested in duplicate.

Ferritin complex purification

The ferritin complex purification procedure was adapted from (Cham et al., 1985), with slight modifications. Either one 15-cm dish of Δ3RE cells grown in normal media or eight 15-cm dishes of wild-type HepG2 cells that had been treated with 50 ng/mL FAC for 24 hours were harvested, weighed, and lysed in 4x weight/volume NP40 lysis buffer (50 mM HEPES-KOH pH=7.5, 150 mM KCl, 2 mM EDTA, 0.5% Nonidet P-40 alternative, 0.5 mM DTT, 1 Complete EDTA-free Protease Inhibitor Cocktail tablet per 10 mL of buffer). Samples were incubated on ice for ten minutes and then centrifuged for 10 minutes at 21,000xg at 4 °C. Samples were diluted in 1:2 phosphate buffered saline (PBS), and methanol was added to the diluted lysate to a final concentration of 40% (v/v). The sample was then heated to 75 °C for 10 min. After cooling on ice for 5 min, the samples were centrifuged in a microfuge 20R at 1,251xg RPM for 15 min at 4°C. The resulting supernatant was collected and concentrated using a 100k MW cutoff Amicon filter (Cat.# UFC510024) by centrifugation for 10 min at 14000xg. The sample was washed once with PBS and spun for an additional 4 min at 14000xg. The sample was then collected by inverting the column and centrifuging the sample for 2 min at 1000xg at 4 °C. All samples collected were brought to a final volume

of 80 µL with PBS. The purity of the sample was determined by running the sample on a native gel (Thermo Fisher Scientific, Cat.# XP04200BOX) followed by Coomassie staining.

Western blots

The following antibodies were used for Western blot analysis: anti-EIF3B (Bethyl A301-761A) at 1:1000; anti-FTL (Abcam, ab69090) at 1:800; anti-FTH (Santa Cruz, sc-25617) at 1:400; anti-IRP1 (Abbexa, abx004618) at 1:400; anti-IRP2 (Abcam, ab129069) at 1:800; and anti-b-Actin (Abcam, ab8227) at 1:1000.

Mathematical Modeling of IRP and eIF3 co-occupancy on *FTL* mRNA

We tested a mathematical model in which IRP and eIF3 do not bind simultaneously to the same *FTL* mRNA. This model thus includes three possible states of the *FTL* mRNA: the fraction bound solely by IRP (x_1), the fraction bound solely by eIF3 (x_2), and the remainder of the mRNA, which is unbound by either factor (x_3) (Figure 2 – figure supplement 2). The model also assumes that the mutations introduced into *FTL* mRNA do not affect the translational efficiency of unbound mRNA species, i.e. translation of x_3 is identical for all 4 mRNAs. The translational efficiency of IRP-bound mRNA (y_1) and eIF3-bound mRNA (y_2) ranges from fully repressed (y = 0) to completely unbound and derepressed (y = 1). Thus, the translational efficiency for the bound populations (x_1 and x_2) is less than 1, while the translational efficiency of x_3 is equal to 1. We also include the parameters α and β to account for changes in the distribution, or shifts, of previously bound mRNA (x_2 *and* x_1) to new populations ($0 \leq \alpha + \beta \leq 1$). Taken

together, 4 overall equations can then represent the luciferase output of each *FTL* mRNA:

(1) $\text{FTL} = y_1 x_1 + y_2 x_2 + x_3$

(2) $\Delta\text{3RE} = y_1 (x_1 + \alpha) + x_2 - \alpha + x_3$

(3) $\text{Loop} = x_1 - \beta + y_2 (x_2 + \beta) + x_3$

(4) $\text{Double} = x_1 + x_2 + x_3$

Here, FTL represents the luciferase readout of wild-type *FTL* mRNA, Δ3RE the luciferase readout of *FTL* mRNA with the Δ3RE mutation, Loop the luciferase readout of *FTL* mRNA with the IRE loop mutation, and Double the luciferase readout of FTL mRNA with both the Δ3RE and Loop mutations. In order to solve this system of equations we proceeded to use experimentally determined values as seen in Figure 2F. We assume the Δ3RE and Loop mutations disrupt regulation by the respective factor (IRP or eIF3) completely, consistent with the biochemical results in Figure 4. In these cases, both y_1 and y_2 revert to a value of 1, i.e. the same translational efficiency of x_3.

To reduce the number of variables, we rearranged equation (1) with normalized luciferase values ($x_3 = 1 - y_1 x_1 - y_2 x_2$) and substituted it into equations (2) through (4)

(5) $\Delta\text{3RE} = y_1 (x_1 + \text{a}) + x_2 - \alpha + 1 - y_1 x_1 - y_2 x_2 \rightarrow 1 + y_1 \alpha - \alpha + (1 - y_2) x_2$

(6) $\text{Loop} = x_1 - \beta + y_2 (x_1 + \beta) + 1 - y_1 x_1 - y_2 x_2 \rightarrow 1 + y_2 \beta - \beta + (1 - y_1) x_1$

(7) $\text{Double} = x_1 + x_2 + 1 - y_1 x_1 - y_2 x_2 \rightarrow 1 + (1 - y_1) x_1 + (1 - y_2) x_2$

Further rearrangement and substitution of Δ3RE and Loop into equation (7) yields:

(8) $(1 - y_2)\, x_2 = \Delta 3\mathrm{RE} - 1 - y_1 \alpha + \alpha$

(9) $(1 - y_1)\, x_1 = \mathrm{Loop} - 1 - y_2 \beta + \beta$

(10) $Double = \mathrm{Loop} + \Delta 3\mathrm{RE} + (\alpha + \beta - y_1 \alpha - y_2 \beta - 1)$

Given the measured luciferase values (Figure 2F), the above model, which assumes IRP and eIF3 do not bind simultaneously to the same *FTL* mRNA, is inconsistent with the data, even accounting for measurement error.

Refer to equation (10):

$41.8\ (\pm 6.5) > 12.5\ (\pm 2.9) + 4.4\ (\pm 0.4) + (\alpha + \beta - y_1 \alpha - y_2 \beta - 1)$

$41.8\ (\pm 6.5) > 16.9\ (\pm 2.9) + (\alpha + \beta - y_1 \alpha - y_2 \beta - 1)$

Thus, IRP and eIF3 likely can act in *cis* on *FTL* mRNAs.

Figures:

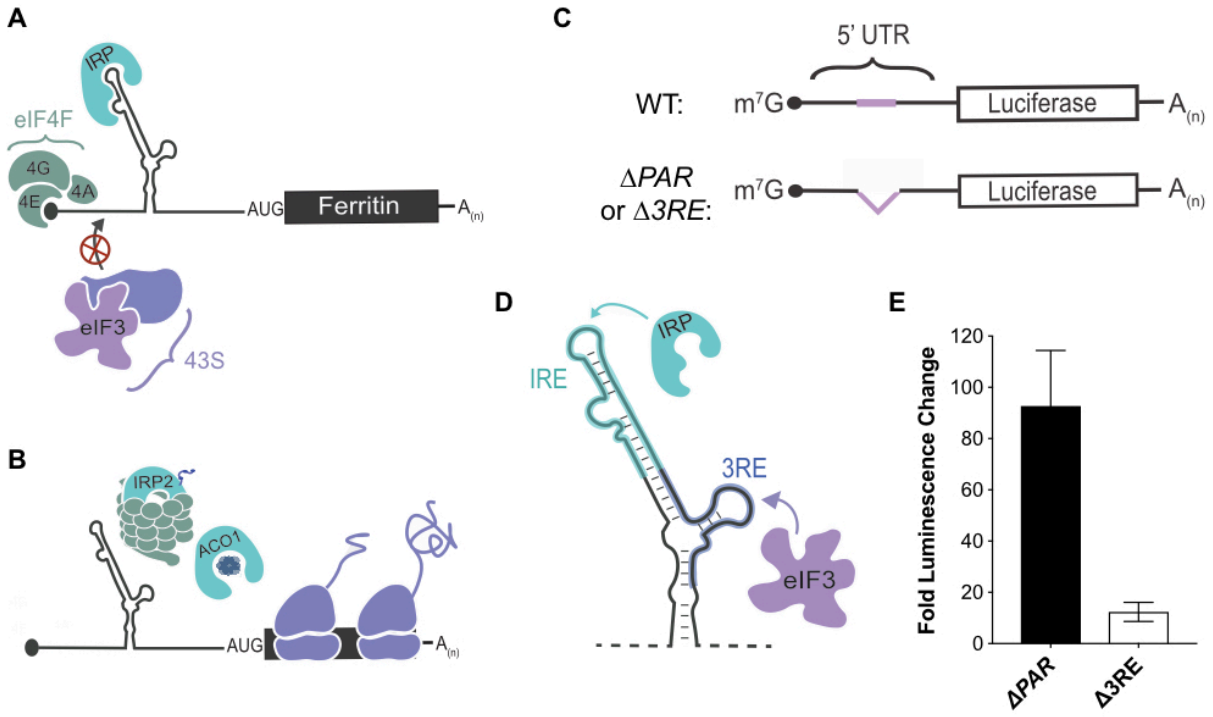

Figure 1. Post-transcriptional regulation of *FTL* mRNA. A, B) Iron-responsive regulation mediated by binding of Iron Response Proteins (IRPs) to Iron Response Element (IRE) RNA structures in the 5'-UTR in (A) low iron conditions and (B) high iron conditions. In high iron, IRP2 is degraded by the proteasome, whereas IRP1 binds an iron-sulfur cluster to form the enzyme Aconitase (ACO1). C) General schematic of the luciferase reporter mRNAs. The eIF3 PAR-CLIP site in *FTL* mRNA spans nucleotides 53-76 (Lee et al., 2015) and the 3RE region spans nucleotides 58-90. D) Schematic of

the IRP and eIF3 interaction sites on the experimentally-determined secondary structure of *FTL* mRNA (Martin et al., 2012). E) Luciferase activity in HepG2 cells transfected with luciferase reporter mRNAs, normalized to luciferase luminescence from mRNA with wild-type *FTL* 5'-UTR. The results show a representative biological replicate, each with three technical replicate transfections, with error bars representing the standard deviation of the mean. Technical replicates involved mRNA transfections used with the same cell sample. The three biological replicates used different samples of cells on different days.

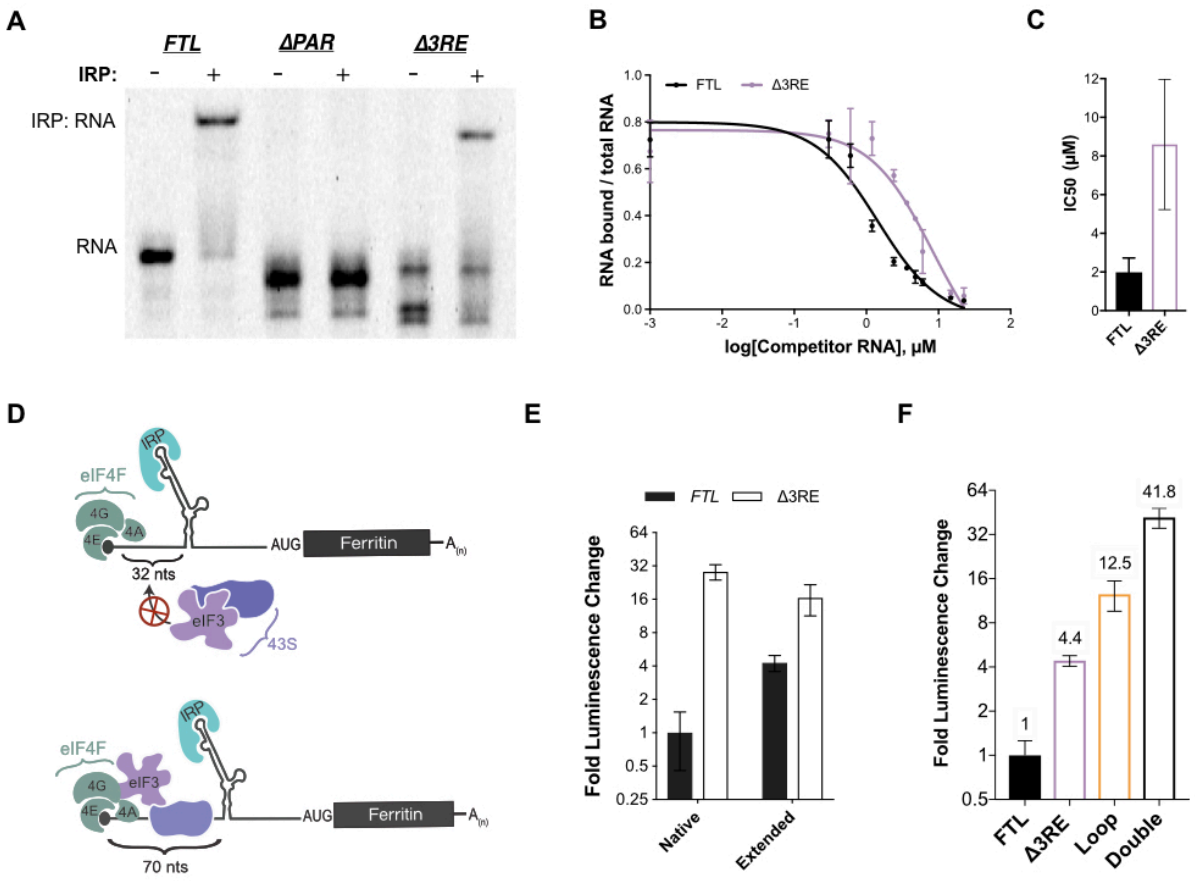

Figure 2. Maintenance of 5'-cap and IRP-dependent regulation of 3RE deletions in the *FTL* 5'-UTR. A) Representative native RNA gel shift showing IRP1 binding activity. Near IR (NIR) labeled RNAs corresponding to the full-length WT *FTL* 5'-UTR and the *FTL* 5'-UTR with deletions of the predicted eIF3 interaction site were incubated with recombinant IRP1, and resolved on a native polyacrylamide gel. B) Dose-response curve of two RNA competition assays, based on gel shifts of NIR-labeled WT IRE-containing RNA, with WT or Δ3RE RNAs serving as cold competitors. Fold excess of competitors extended up to 75,000x. Error bars represent standard deviations for each

concentration of competitor. C) Calculated IC_{50} values using Prism 7 of the various competitor RNAs, based on the data in (B), with error bars representing the standard deviation from the mean IC_{50} value. N.A., the IC_{50} value could not be determined for the Loop mutant due to lack of any detectable competition. D) Schematics showing the effect of increasing the distance of the IRE from the 5'-cap on IRP regulation of translation initiation (Goossen and Hentze, 1992), (Muckenthaler et al., 1998). E) The luciferase activity of HepG2 cells transfected with mRNAs containing the native and extended spacing between the 5'-cap and IRE, with or without the 3RE site, normalized to the luciferase luminescence of cells transfected with WT *FTL* mRNA with native spacing from the 5'-cap. The results are of three technical replicate mRNA transfections from one of three biological replicates, with error bars representing the standard deviation of the mean. F) The luciferase activity of HepG2 cells transfected with mRNAs containing the native and various combinations of eIF3 (Δ3RE) and IRP (Loop) disrupting mutations in HepG2 cells, normalized to the luciferase luminescence of cells transfected with WT *FTL* mRNA with native spacing from the 5'-cap. The results are from six independent transfections, with error bars representing the standard deviation of the mean. This experiment was performed with a shortened incubation time of 6 hr to keep readouts for various mutant constructs in linear range (Bert et al., 2006).

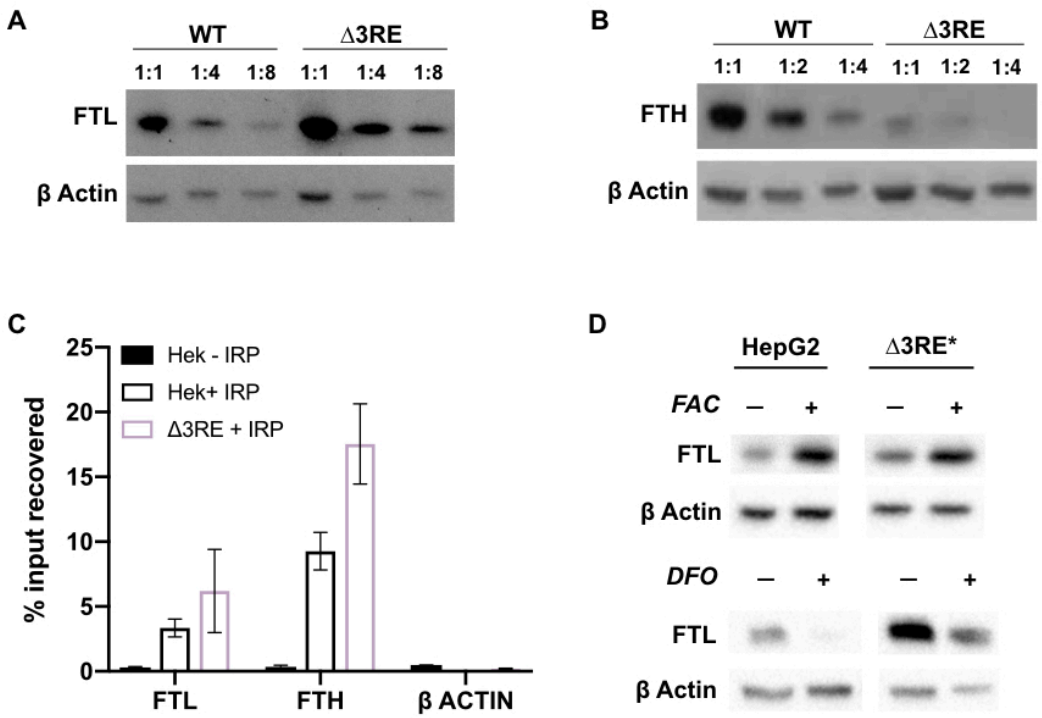

Figure 3. Physiological effects of the endogenous removal of the 3RE repressive element. A,B) Representative Western blots of (A) FTL and (B) FTH levels in the edited (Δ3RE) and WT HepG2 cells under normal iron conditions. Serial dilutions were used in order to better visualize the significance of the changes in FTL and FTH protein abundance. (C) Determination of IRP1 binding to *FTL* mRNA in WT (Hek + IRP) and Δ*3RE* (Δ3RE + IRP) HEK293T cells via FLAG immunoprecipitation (IP) followed by RNA extraction and RT-qPCR. The *ACTB* mRNA was used to control for nonspecific binding to FLAG-tagged IRP. Hek – IRP reflects cells that were not transiently transfected, but were carried through the IP and following experiments. Error bars represent the standard deviation of triplicate measurements from representative IP reactions. (D) Representative Western blots of FTL levels in the edited (Δ3RE) and WT HepG2 cells under high or low iron conditions. Iron donor treatment with FAC at 50 µg/mL for 24 hr,

and Iron chelation treatment with DFO at 50 μM for 48 hr. The asterisk (*) indicates that lysate from Δ3RE cells were diluted two-fold, due to the higher overall levels of FTL in these cells. All blots are representative of 3 or more replicates.

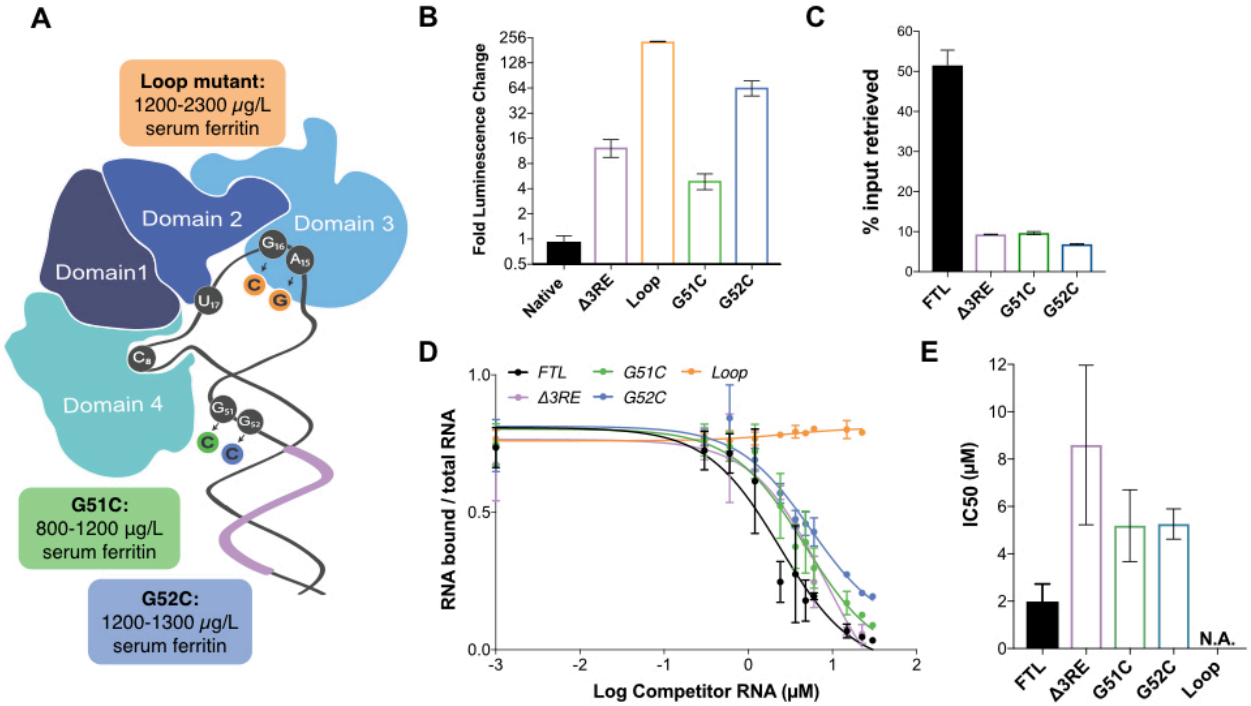

Figure 4. Role of eIF3 in select cases of Hyperferritinemia. A) Diagram of IRP binding to the IRE in *FTL* mRNA (Anderson and McLaren, 2012). Hyperferritinemia mutations are highlighted in orange (Cazzola et al., 1997), green (Camaschella et al., 2000), and blue (Luscieti et al., 2013) with their corresponding serum ferritin levels listed. The 3RE is indicated in purple. Nucleotides that directly interact with the IRP are also identified (i.e. A15, G16, U17). B) Luciferase activity of HepG2 cells transfected with mRNAs encoding the WT *FTL* 5'-UTR or various hyperferritinemia mutations, normalized to WT *FTL* reporter luciferase luminescence. The results shown are of three technical replicate mRNA transfections from one of three biological replicates, with error bars representing the standard deviation of the mean. C) Binding of eIF3 to luciferase reporter mRNAs with WT or mutant forms of the *FTL* 5'-UTR, using EIF3B immunoprecipitation (IP), followed by RNA extraction and RT-qPCR. Cells were harvested 8 hrs post-transfection. Data are shown as the percent in the IP compared input levels. Error bars are the standard deviation of the mean of duplicate qPCR

measurements from a representative IP. D) Dose-response curve of RNA competition assays, based on gel shifts of NIR-labeled WT IRE-containing RNA, with WT, G51C, G52C, or Loop mutant (A15G/G16C) RNAs serving as cold competitors. Fold excess of competitors extended up to 100,000x. Error bars represent standard deviations for each concentration of competitor. E) The calculated IC_{50} values of the various competitor RNAs, based on the data in (D), with error bars representing the standard deviation from the mean IC_{50} value. N.A., the IC_{50} value could not be determined for the Loop mutant due to lack of any detectable competition. Note that the data for Δ3RE in panels (D) and (E) are from Figure 2B, 2C, measured in duplicate. The remaining experiments in (D) and (E) were carried out in triplicate.

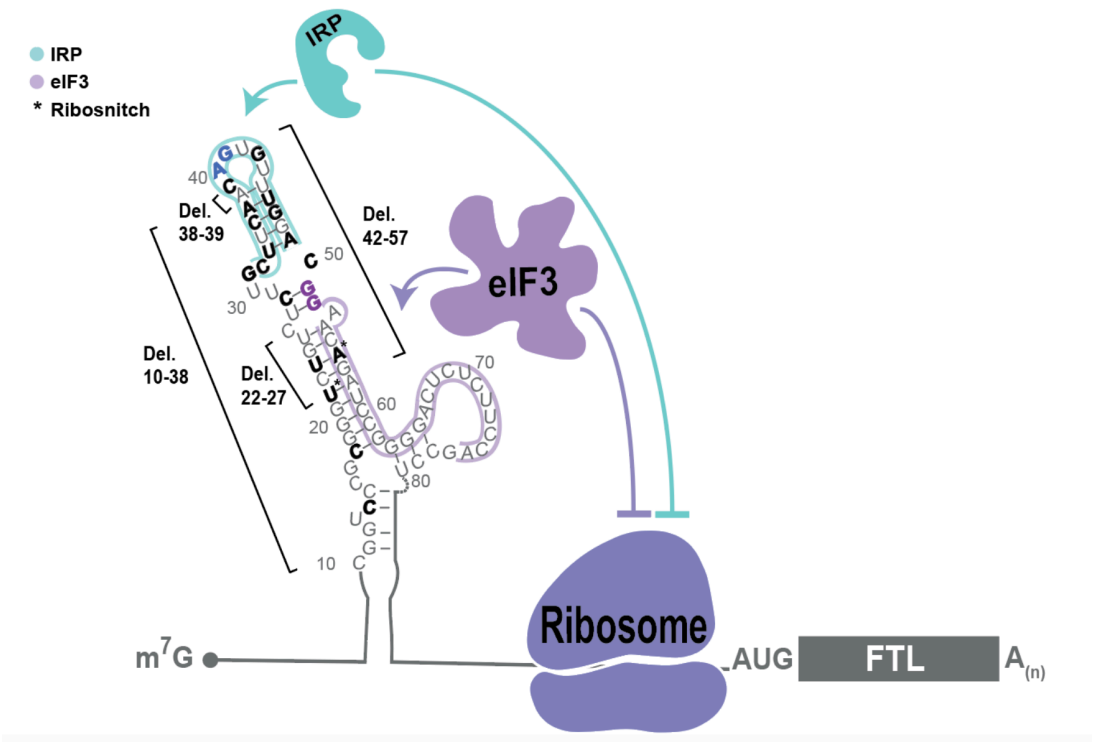

Figure 5. Model of post-transcriptional regulation of *FTL* mRNA. IRPs repress *FTL* mRNA translation in an iron-dependent manner, whereas eIF3 represses *FTL* translation in an iron-independent manner. Coordination between IRP repression and eIF3 repression may differ by cell and tissue context. Various hyperferritinemia mutations (bolded) listed in the literature are mapped on the experimentally-determined secondary structure of the *FTL* mRNA 5'-UTR (Martin et al., 2012), (Luscieti et al., 2013). The minimal annotation of the IRE is denoted by with a blue outline and the eIF3 PAR-CLIP defined interaction site is denoted with a purple outline. Mutations that disrupt IRP binding used in this study and determined here to disrupt eIF3 binding are bolded in blue and purple, respectively. The asterisk (*) indicates nucleotides identified as ribosnitches (Martin et al., 2012).

Supplemental Figures

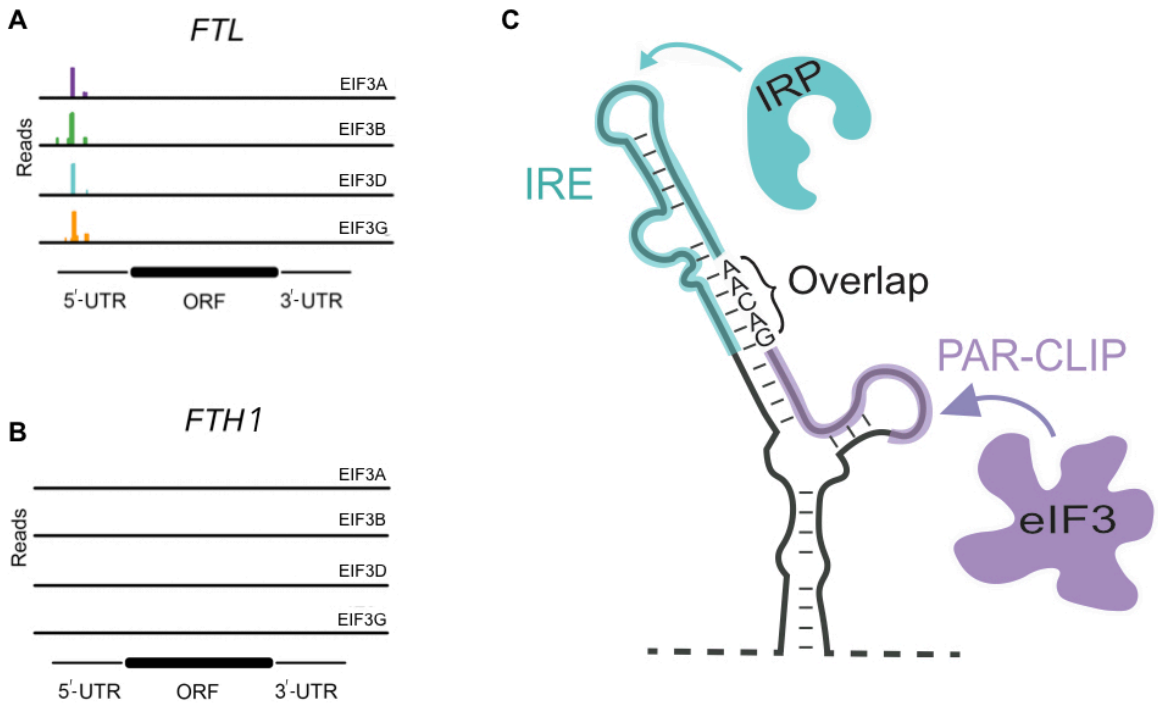

Figure 1 – figure supplement 1. Sites of eIF3 interaction with *FTL* and *FTH1* mRNAs. A, B) eIF3 PAR-CLIP cluster identified for (A) *FTL* but missing in (B) *FTH1* (Lee et al., 2015). **C)** Mapping of the IRP and PAR-CLIP derived eIF3 interaction sites on the secondary structure of the 5'-UTR in *FTL* mRNA, determined by chemical probing (Martin et al., 2012).

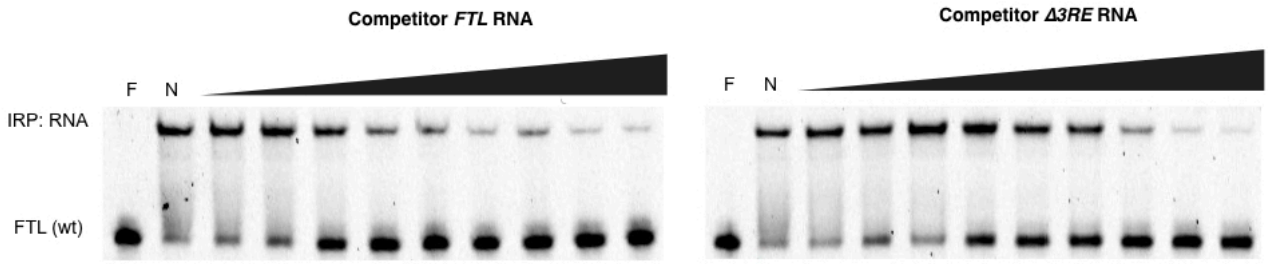

Figure 2 – figure supplement 1. Native gels resolving RNA-IRP1 complexes formed after competition experiments. Near IR (NIR) labeled RNA corresponding to the full-length WT *FTL* 5'-UTR were incubated with recombinant IRP1 and increasing molar excess concentrations of unlabeled competitor *FTL* or Δ*3RE* RNA (1,000x, 2,000x, 4,000x, 8,000x, 12,000x, 16,000x, 20,000x, 50,000x, 75,000x), as indicated. F, lane with only NIR-labeled *FTL* RNA; N, no addition of competitor RNA to the NIR-RNA-IRP1 complex. Representative gels are shown.

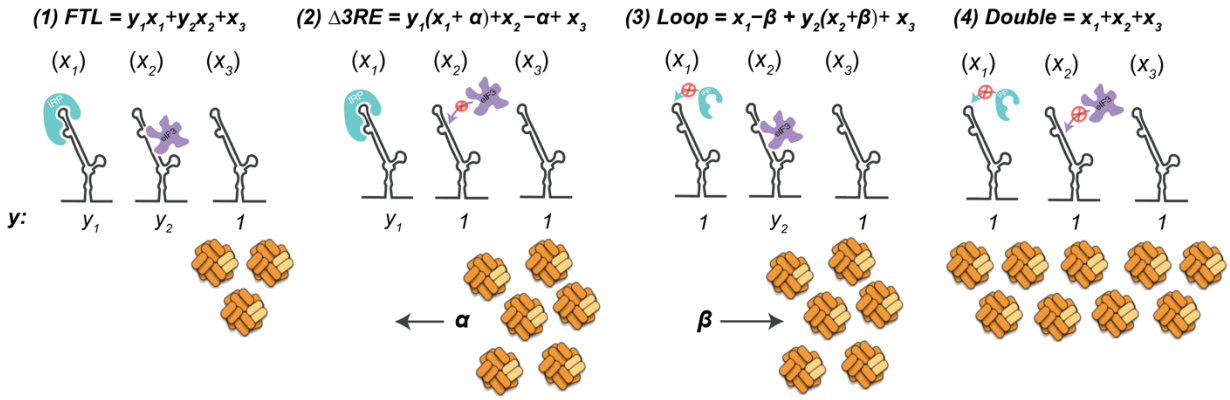

Figure 2 – figure supplement 2. Mathematical modeling of IRP and eIF3 co occupancy on *FTL* mRNA Schematic for mathematical modeling based on luciferase activity shown in Fig. 2F which demonstrates that IRP and eIF3 seem to work synergistically rather than exclusively. x_1 represents the fraction of *FTL* mRNA bound by IRP. x_2 represents the fraction of *FTL* mRNA bound by eIF3. x_3 represents the fraction of unbound *FTL* mRNA. α and β represent a fraction of the previously bound mRNA populations x_2 and x_1 respectively.

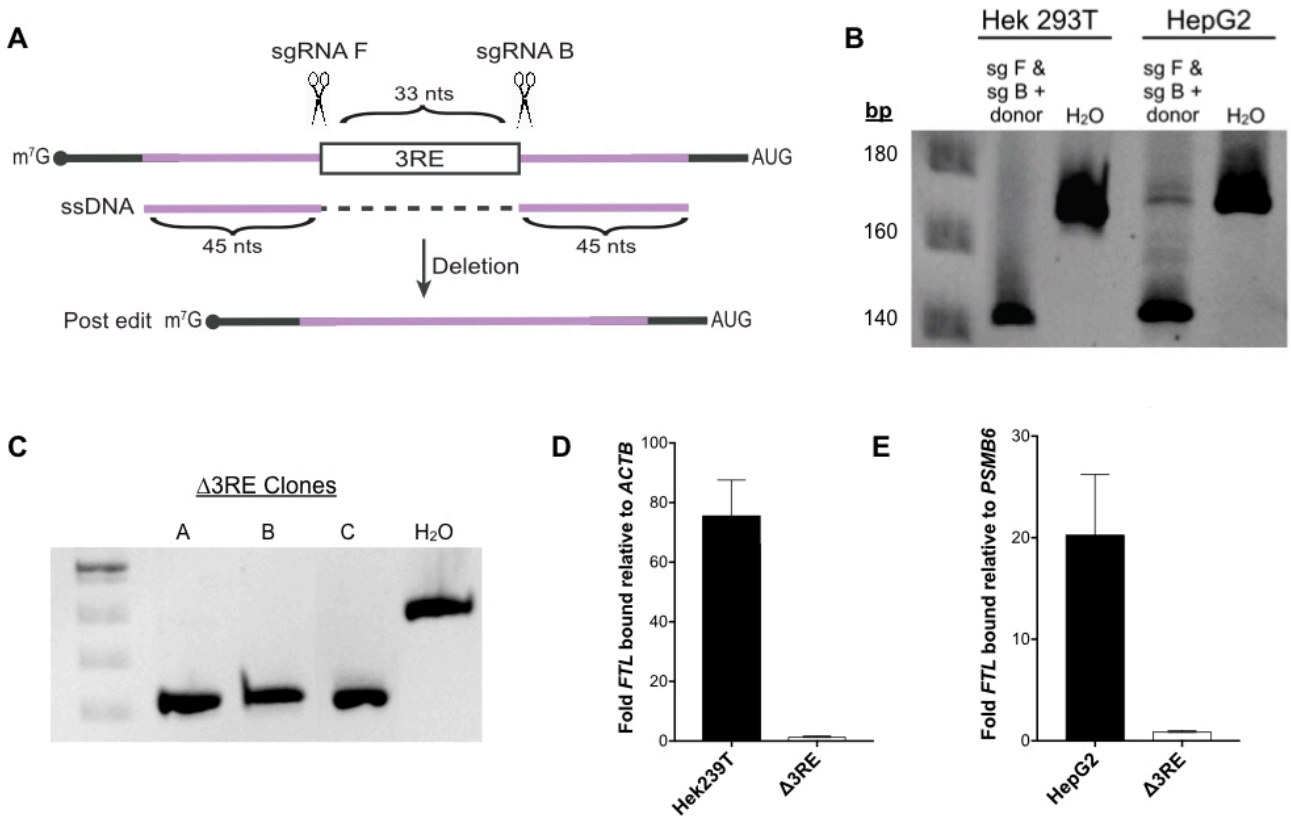

Figure 3 – figure supplement 1. CRISPR-Cas9 editing to remove the proposed eIF3-*FTL* interaction site. A) CRISPR-Cas9 RNP editing schematic in which two sgRNAs target sequences immediately adjacent to the 3RE. Reactions were supplemented with 90-nt ssDNA that had full homology to the intended edited sequence. B) Editing efficiency in both HEK293T and HepG2 cells, based on PCR of the region of interest and analysis on a native polyacrylamide gel. C) Three successfully edited HepG2 clonal populations, as determined by sequencing the *FTL* locus. D, E) Determination of the preferential binding of eIF3 to *FTL* mRNA via EIF3B immunoprecipitation (IP) followed by RNA extraction and RT-qPCR in both (D) HEK293T and (E) HepG2 cell lines. Control mRNAs used to normalize IPs were *PSMB6*

and *ACTB*. Error bars represent the standard deviation of duplicate qPCR measurements from representative IP reactions.

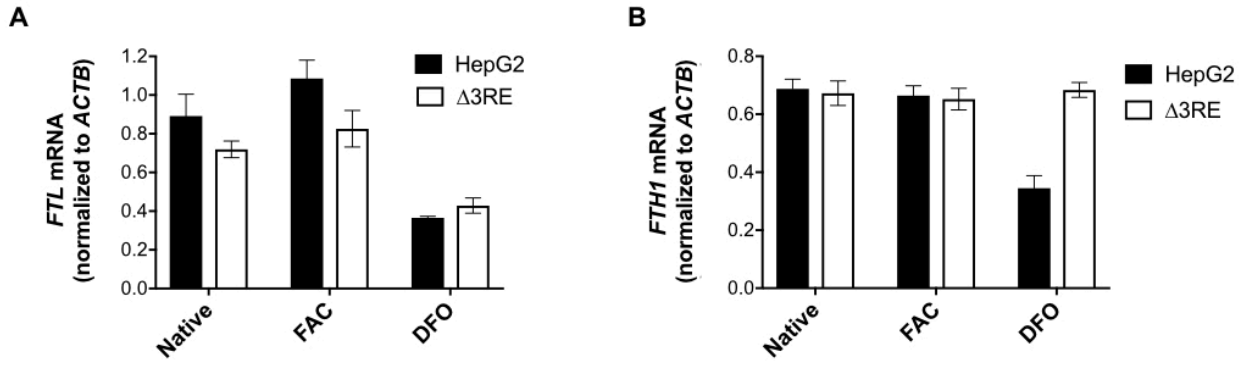

Figure 3 – figure supplement 2. mRNA levels in edited cell lines. A, B) mRNA levels of either (A) *FTL* or (B) *FTH1* as determined by RNA extraction from HepG2 (solid black bars) or HepG2 Δ3RE (black outlined bars) cells and RT-qPCR. The mRNA levels for *FTL* and *FTH1* were normalized to *ACTB* mRNA. Cells were grown in normal media, 50 µg/mL FAC treatment for 24 hr, or 200 µM DFO treatment for 24 hr. The results are from two or three technical replicate qPCR readouts that reflect the data from two biological replicates, with error bars representing the standard deviation of the mean.

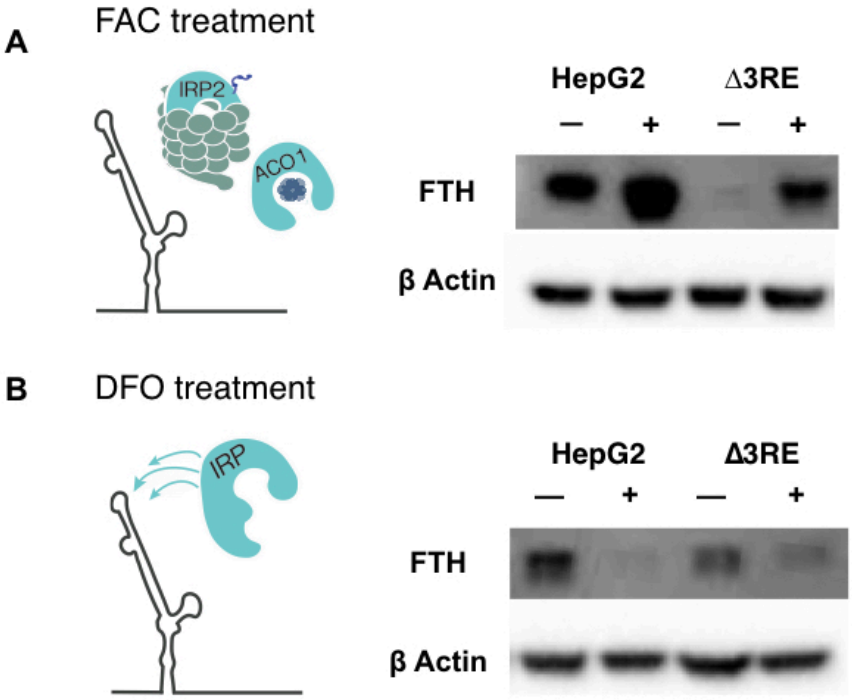

Figure 3 – figure supplement 3. Physiological effects of the endogenous removal of the 3RE on FTH protein levels. A, B) Representative Western blots of FTH levels in the edited (Δ3RE) and WT HepG2 cells under various iron conditions. (A) Iron donor treatment with FAC at 50 µg/mL for 24hr; (B) Iron chelation treatment with DFO at 200 µM for 24 hr.

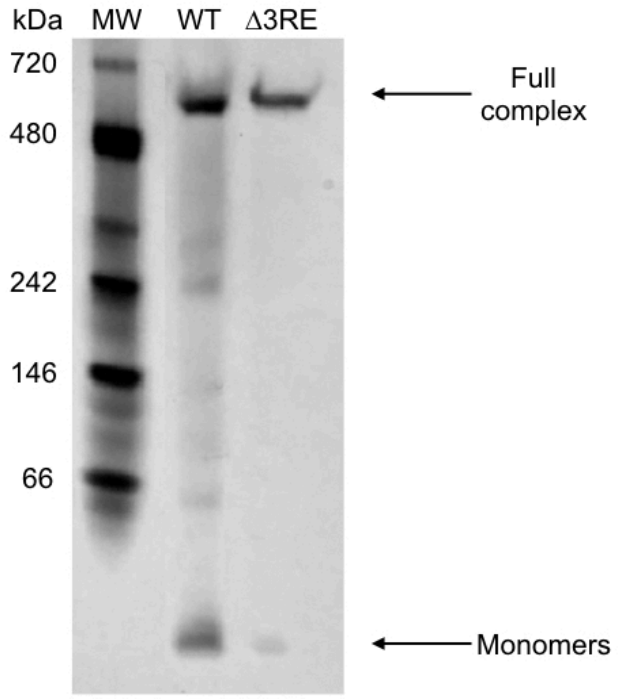

Figure 3 – figure supplement 4. Analysis of the ferritin complex upon deletion of the 3RE in FTL mRNA. Representative native 4-12% gradient Tris-Glycine gel resolving ferritin complexes purified using methanol, from either 8x 15-cm dishes of WT HepG2 cells treated with 50 µg/mL FAC for 24 hrs or a single 15-cm dish of Δ3RE HepG2 cells under normal media conditions.

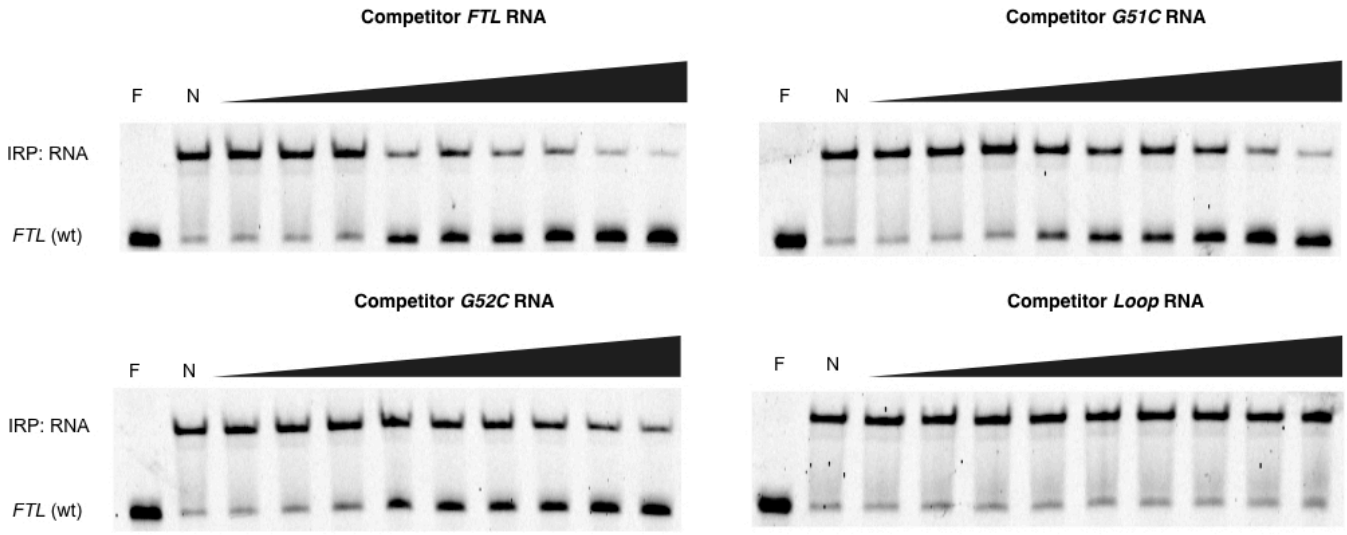

Figure 4 – figure supplement 1. Native gels resolving RNA-IRP1 complexes formed after competition experiments with hyperferritinemia-related RNAs. Near IR (NIR) labeled RNA corresponding to the full-length WT FTL 5'-UTR were incubated with recombinant IRP1 and increasing molar excess concentrations of unlabeled competitor RNAs (1,000x, 2,000x, 4,000x, 8,000x, 12,000x, 16,000x, 20,000x, 50,000x, 75,000x), as indicated. F, lane with only NIR-labeled FTL RNA; N, no addition of competitor RNA to the NIR-RNA-IRP1 complex. Representative gels are shown.

Author Contributions

MCPH designed the main conceptual ideas and carried out the majority of the experiments. MCPH, DTM and JHDC conceived the project. DNS assisted in carrying out experiments related to screening and obtaining clonal cell lines, as well as plasmid construct generation. MGJ aided in plasmid construct generation and accessory biochemical experiments. ASYL collaborated in early stage experimental design. JHDC and NTI supervised and aided in the planning of the overall direction for the project. MCPH and JHDC drafted the manuscript. All authors edited the manuscript.

Acknowledgments: We are immensely grateful to Bruno Martinez for providing us with purified IRP1, Luisa Arake De Tacca for help optimizing the eIF3 immunoprecipitations and for many constructive discussions, Zoe Watson for discussions on modeling, Hector Nolla for help with flow cytometry and single cell sorting, and Alison Killilea and the Berkeley tissue culture facility for cells and advice.

Funding:

P50 GM102706/GM/NIGMS NIH HHS/United States

R01 GM065050/GM/NIGMS NIH HHS/United States

AHA predoctoral fellowship 16PRE30140013/United States

References

Anderson GJ, McLaren GD. 2012. Iron physiology and pathophysiology in humans. Humana Press. doi:10.1007/978-1-60327-485-2

Ascano M, Hafner M, Cekan P, Gerstberger S, Tuschl T. 2011. Identification of RNA-protein interaction networks using PAR-CLIP. *WIREs RNA* **3**:159–177. doi:10.1002/wrna.1103

Basilion JP, Rouault TA, Massinople CM, Klausner RD, Burgess WH. 1994. The iron-responsive element-binding protein: localization of the RNA-binding site to the aconitase active-site cleft. *Proc Natl Acad Sci USA* **91**:574–578.

Bert AG, Grépin R, Vadas MA, Goodall GJ. 2006. Assessing IRES activity in the HIF-1alpha and other cellular 5' UTRs. *RNA* **12**:1074–1083. doi:10.1261/rna.2320506

Camaschella, Zecchina, Lockitch, Roetto, Campanella, Arosio, Levi. 2000. A new mutation (G51C) in the iron-responsive element (IRE) of l-ferritin associated with hyperferritinaemia-cataract syndrome decreases the binding affinity of the mutated IRE for iron-regulatory proteins. *British Journal of Haematology* **108**:480–482. doi:10.1046/j.1365-2141.2000.01920.x

Carvalho H, Meneghini R. 2008. Increased expression and purification of soluble iron-regulatory protein 1 from Escherichia coli co-expressing chaperonins GroES and GroEL. *Braz J Med Biol Res* **41**:270–276. doi:10.1590/S0100-879X2008005000009

Cazzola M, Bergamaschi G, Tonon L, Arbustini E, Grasso M, Vercesi E, Barosi G, Bianchi PE, Cairo G, Arosio P. 1997. Hereditary hyperferritinemia-cataract syndrome: relationship between phenotypes and specific mutations in the iron-responsive element of ferritin light-chain mRNA. *Blood* **90**:814–821.

Cham BE, Roeser HP, Nikles A, Ridgway K. 1985. A procedure for the purification of ferritin from human liver by heating a methanol-treated homogenate. *Anal Biochem* **151**:561–565.

Chen JL-Y, Lucas JE, Schroeder T, Mori S, Wu J, Nevins J, Dewhirst M, West M, Chi J-T. 2008. The Genomic Analysis of Lactic Acidosis and Acidosis Response in Human Cancers. *PLoS Genet* **4**:e1000293–16. doi:10.1371/journal.pgen.1000293

Cozzi A, Corsi B, Levi S, Santambrogio P, Biasiotto G, Arosio P. 2004. Analysis of the biologic functions of H- and L-ferritins in HeLa cells by transfection with siRNAs and cDNAs: evidence for a proliferative role of L-ferritin. *Blood* **103**:2377–2383. doi:10.1182/blood-2003-06-1842

Fillebeen C, Wilkinson N, Pantopoulos K. 2014. Electrophoretic Mobility Shift Assay (EMSA) for the Study of RNA-Protein Interactions: The IRE/IRP Example. *JoVE* 1–9. doi:10.3791/52230

Goforth JB, Anderson SA, Nizzi CP, Eisenstein RS. 2009. Multiple determinants within iron-responsive elements dictate iron regulatory protein binding and regulatory hierarchy. *RNA* **16**:154–169. doi:10.1261/rna.1857210

Goossen B, Hentze MW. 1992. Position is the critical determinant for function of iron-responsive elements as translational regulators. *Mol Cell Biol* **12**:1959–1966.

Hafner M, Landthaler M, Burger L, Khorshid M, Hausser J, Berninger P, Rothballer A, Ascano M, Jungkamp A-C, Munschauer M, Ulrich A, Wardle GS, Dewell S, Zavolan M, Tuschl T. 2010. PAR-CliP - A Method to Identify Transcriptome-wide the Binding Sites of RNA Binding Proteins. *JoVE* 1–5. doi:10.3791/2034

Harrison PM, Arosio P. 1996. The ferritins: molecular properties, iron storage function and cellular regulation. *Biochim Biophys Acta* **1275**:161–203. doi:10.1016/0005-2728(96)00022-9

Kim S, Kim D, Cho SW, Kim J, Kim JS. 2014. Highly efficient RNA-guided genome editing in human cells via delivery of purified Cas9 ribonucleoproteins. *Genome Research* **24**:1012–1019. doi:10.1101/gr.171322.113

Knovich MA, Storey JA, Coffman LG, Torti SV, Torti FM. 2009. Ferritin for the clinician. *Blood Reviews* **23**:95–104. doi:10.1016/j.blre.2008.08.001

Kohn M, Lederer M, Wachter K, Huttelmaier S. 2010. Near-infrared (NIR) dye-labeled RNAs identify binding of ZBP1 to the noncoding Y3-RNA. *RNA* **16**:1420–1428. doi:10.1261/rna.2152710

Kong YW, Cannell IG, de Moor CH, Hill K, Garside PG, Hamilton TL, Meijer HA, Dobbyn HC, Stoneley M, Spriggs KA, Willis AE, Bushell M. 2008. The mechanism of micro-RNA-mediated translation repression is determined by the promoter of the target gene. *Proc Natl Acad Sci USA* **105**:8866–8871. doi:10.1073/pnas.0800650105

Kranzusch PJ, Lee ASY, Wilson SC, Solovykh MS, Vance RE, Berger JM, Doudna JA. 2014. Structure-Guided Reprogramming of Human cGAS Dinucleotide Linkage Specificity. *Cell* **158**:1011–1021. doi:10.1016/j.cell.2014.07.028

Lee ASY, Kranzusch PJ, Cate JHD. 2015. eIF3 targets cell-proliferation messenger RNAs for translational activation or repression. *Nature* **522**:111–114. doi:10.1038/nature14267

Lee ASY, Kranzusch PJ, Doudna JA, Cate JHD. 2016. eIF3d is an mRNA cap-binding protein that is required for specialized translation initiation. *Nature* **536**:96–99. doi:10.1038/nature18954

Linder MC. 2013. Mobilization of stored iron in mammals: a review. *Nutrients* **5**:4022–4050. doi:10.3390/nu5104022

Liu H-D, Li W, Chen Z-R, Zhou M-L, Zhuang Z, Zhang D-D, Zhu L, Hang C-H. 2012. Increased expression of ferritin in cerebral cortex after human traumatic brain injury. *Neurol Sci* **34**:1173–1180. doi:10.1007/s10072-012-1214-7

Lizio M, Harshbarger J, Shimoji H, Severin J, Kasukawa T, Sahin S, Abugessaisa I, Fukuda S, Hori F, Ishikawa-Kato S, Mungall CJ, Arner E, Baillie JK, Bertin N, Bono H, de Hoon M, Diehl AD, Dimont E, Freeman TC, Fujieda K, Hide W, Kaliyaperumal R, Katayama T, Lassmann T, Meehan TF, Nishikata K, Ono H, Rehli M, Sandelin A, Schultes EA, 't Hoen PAC, Tatum Z, Thompson M, Toyoda T, Wright DW, Daub CO, Itoh M, Carninci P, Hayashizaki Y, Forrest ARR, Kawaji H, FANTOM consortium. 2015. Gateways to the FANTOM5 promoter level mammalian expression atlas. *Genome Biol* **16**:22. doi:10.1186/s13059-014-0560-6

Luscieti S, Tolle G, Aranda J, Campos CB, Risse F, Morán É, Muckenthaler MU, Sánchez M. 2013. Novel mutations in the ferritin-L iron-responsive element that only mildly impair IRP binding cause hereditary hyperferritinaemia cataract syndrome. *Orphanet Journal of Rare Diseases* **8**:1–10. doi:10.1186/1750-1172-8-30

Martin JS, Halvorsen M, Davis-Neulander L, Ritz J, Gopinath C, Beauregard A, Laederach A. 2012. Structural effects of linkage disequilibrium on the transcriptome. *RNA* **18**:77–87. doi:10.1261/rna.029900.111

Millonig G, Muckenthaler MU, Mueller S. 2010. Hyperferritinaemia-cataract syndrome: worldwide mutations and phenotype of an increasingly diagnosed genetic disorder. *Hum Genomics* **4**:250–262. doi:10.1186/1479-7364-4-4-250

Mokany E, Tan YL, Bone SM, Fuery CJ, Todd AV. 2013. MNAzyme qPCR with Superior Multiplexing Capacity. *Clinical Chemistry* **59**:419–426. doi:10.1373/clinchem.2012.192930

Morikawa K, Oseko F, Morikawa S. 2009. A Role for Ferritin in Hematopoiesis and the Immune System. *Leukemia & Lymphoma* **18**:429–433. doi:10.3109/10428199509059641

Muckenthaler M, Gray NK, Hentze MW. 1998. IRP-1 binding to ferritin mRNA prevents the recruitment of the small ribosomal subunit by the cap-binding complex eIF4F. *Mol Cell* **2**:383–388.

Paraskeva E, Gray NK, Schläger B, Wehr K, Hentze MW. 1999. Ribosomal pausing and scanning arrest as mechanisms of translational regulation from cap-distal iron-responsive elements. *Mol Cell Biol* **19**:807–816.

Ramlee MK, Yan T, Cheung AMS, Chuah CTH, Li S. 2018. High-throughput genotyping of CRISPR/Cas9-mediated mutants using fluorescent PCR-capillary gel electrophoresis. *Nature Publishing Group* 1–13. doi:10.1038/srep15587

Recalcati S, Invernizzi P, Arosio P, Cairo G. 2008. New functions for an iron storage protein: The role of ferritin in immunity and autoimmunity. *Journal of Autoimmunity* **30**:84–89. doi:10.1016/j.jaut.2007.11.003

Reyon D, Tsai SQ, Khayter C, Foden JA, Sander JD, Joung JK. 2012. FLASH assembly of TALENs for high-throughput genome editing. *Nat Biotechnol* **30**:460–465. doi:10.1038/nbt.2170

Sammarco MC, Ditch S, Banerjee A, Grabczyk E. 2008. Ferritin L and H Subunits Are Differentially Regulated on a Post-transcriptional Level. *Journal of Biological Chemistry* **283**:4578–4587. doi:10.1074/jbc.M703456200

Schneider BD, Leibold EA. 2003. Effects of iron regulatory protein regulation on iron homeostasis during hypoxia. *Blood* **102**:3404–3411. doi:10.1182/blood-2003-02-0433

Studier FW. 2005. Protein production by auto-induction in high-density shaking cultures. *Protein Expression and Purification* **41**:207–234. doi:10.1016/j.pep.2005.01.016

Theil EC. 2015. IRE mRNA riboregulators use metabolic iron (Fe2+) to control mRNA activity and iron chemistry in animals. *Metallomics* **7**:15–24. doi:10.1039/C4MT00136B

Theil EC. 1994. Iron regulatory elements (IREs): a family of mRNA non-coding sequences. *Biochem J* **304 (Pt 1)**:1–11.

Walden WE, Selezneva AI, Dupuy J, Volbeda A, Fontecilla-Camps JC, Theil EC, Volz K. 2006. Structure of dual function iron regulatory protein 1 complexed with ferritin IRE-RNA. *Science* **314**:1903–1908. doi:10.1126/science.1133116

Wilkinson N, Pantopoulos K. 2014. The IRP/IRE system in vivo: insights from mouse models. *Front Pharmacol* **5**:176. doi:10.3389/fphar.2014.00176